A Novel Distributed Control Strategy for Optimal Dispatch of Isolated Microgrids Considering Congestion

Jacqueline Llanos, *Member, IEEE*, Daniel E. Olivares, *Member, IEEE*, John W. Simpson-Porco, *Member, IEEE*, Mehrdad Kazerani, *Senior Member, IEEE*, and Doris Sáez, *Senior Member, IEEE*

***Abstract*—This paper presents a novel distributed control strategy for frequency control, congestion management, and optimal dispatch (OD) in isolated microgrids. The proposed strategy drives the distributed generators (DGs) within the microgrid to a dispatch that complies with the Karush–Kuhn–Tucker (KKT) conditions of a linear optimal power flow (OPF) formulation. The controller relies on local power and frequency measurements, information from neighboring DGs, and line-flow measurements transmitted through a communications network. Extensive simulations show a good performance of the controller against sudden changes in the load, congested lines and availability of DGs in the microgrid, and the ability to successfully drive the system to an optimal economic operation.**

***Index Terms*—Distributed control, microgrid, congestion, optimal dispatch.**

I. Introduction

A MICROGRID has been defined as a cluster of Distributed Generation (DG) units, Energy Storage Systems (ESSs), and distributed loads, operated in coordination to reliably supply electricity [1]. A main driver for the deployment of microgrids is to allow seamless integration of DG units.

The microgrid control tasks can be divided into 3 distinctive levels: 1) output current, voltage, and frequency control of DG units (Primary Control), 2) frequency restoration and optimal dispatch of the microgrid (Secondary Control), and 3) coordination of the microgrid with the main grid (Tertiary Control) [2]. Since most DG units require a DC-to-AC power electronic interface, the design of control schemes in the three levels that are applicable to inverter-interfaced units is a must.

Frequency and voltage restoration in a microgrid can be realized using centralized or distributed controller schemes. Recently, there has been a rise in attention to distributed control and its applications in microgrids due to the need for higher reliability and security [3]. For instance, in [4], [5] and [6], the authors propose distributed schemes for restoring frequency and voltage considering active and reactive power sharing among the inverters of DG units in a microgrid. A PI controller proposed in [4] uses the average measured frequency for regulation purposes; however, such approach presents difficulties when outages of DG units occur. On the other hand, a consensus-based controller using distributed-averaging proportional-integral (DAPI) control is proposed in [5], which does not present the aforementioned issue. Also, the constraints related to the voltage magnitudes and angles are incorporated in [6]. While these proposals achieve an adequate operation of the microgrid, they do not consider its optimal economic operation.

The optimal operation of a microgrid is typically obtained by solving an economic dispatch problem under a centralized approach. However, due to the advantages of distributed control approaches, recent works have proposed the use of distributed economic dispatch algorithms based on the decomposition techniques.

The multi-agent system (MAS) is a popular distributed control method, where a consensus algorithm is used for the coordination of agents. For instance, in [7] a MAS has been proposed for the optimal resource management in an isolated microgrid. In [8], frequency regulation and optimal dispatch controls are proposed based on MAS. The incremental cost consensus is frequently used when transmission losses are considered in optimal management [9]–[11]. In [9] an Energy Management System (EMS) based on an incremental cost consensus strategy is presented for optimal dispatch DG units and demand response. The strategy proposed in [11] reaches consensus of lagrangian multipliers using a correction term that ensures demand-supply balance.

Manuscript received May 16, 2018; revised September 14, 2018 and December 5, 2018; accepted March 15, 2019. Date of publication March 28, 2019; date of current version October 30, 2019. This work was supported in part by CONICYT under Grant FONDECYT/1170683 and Grant FONDECYT/1181517, in part by the Complex Engineering Systems Institute under Grant CONICYT/FB0816, and in part by the Solar Energy Research Center SERC-Chile under Grant CONICYT/FONDAP/15110019. The work of J. Llanos was supported by the Ph.D. Scholarship from CONICYT/63140113 Doctorado Nacional para Extranjeros 2014. Paper no. TSG-00746-2018. *(Corresponding author: Daniel E. Olivares.)*

J. Llanos and D. Sáez are with the Department of Electrical Engineering, University of Chile, Santiago 8370451, Chile (e-mail: jllanos@ug.uchile.cl; dsaez@ing.uchile.cl).

D. E. Olivares is with the EE Department, Pontificia Universidad Católica de Chile, Santiago 7820436, Chile, and also with the UC Energy Research Center, Pontificia Universidad Católica de Chile, Santiago 7820436, Chile.

J. W. Simpson-Porco and M. Kazerani are with the Department of Electrical and Computer Engineering, University of Waterloo, Waterloo, ON N2L 3G1, Canada.

Color versions of one or more of the figures in this paper are available online at http://ieeexplore.ieee.org.

Digital Object Identifier 10.1109/TSG.2019.2908128

The optimal distributed control schemes have also been used in bulk power systems. Some applications are presented in [12]–[14] and [15]. In [12] a decentralized optimal frequency control with controllable loads is described. In [13] a distributed optimal frequency control for a power system is proposed, achieving automatic congestion control.

The control of isolated microgrids is more challenging than in grid-connected ones due to a more critical demand-supply balance, and limited controllable assets to solve voltage and overloading problems [1]. Lines overloading, or congestion, can significantly affect the lifetime of the distribution lines and transformers in the microgrid, and the activation of thermal protections could can lead to unsupplied demand [16].

In bulk power systems, the congestion of transmission corridors is typically managed by re-dispatching generation units; however, more a advanced control can also be achieved by phase shifters, line switching, FACTS/HVDC controllers, and even load curtailment [17]. In distribution networks, the problem of congestion management has been mostly approached using demand flexibility [16], [18]–[20], or smart transformers [21]; where the proposed solutions require adding new expensive technology to existing systems, or using distributed optimization techniques.

Recently, in [22], a consensus-based algorithm for frequency regulation in isolated microgrid has been proposed, taking into account the congestion of distribution lines. This work addresses the problem of congestion using a hierarchical approach where the Distribution Network Operator (DNO) sends optimal set points of generation, and a lower-level control changes these set point values for congestion management; therefore, the new set points are not optimal. To the best of the authors' knowledge, the problem of combined congestion management and optimal dispatch in microgrids has not been thoroughly studied in the existing literature.

In [23], a distributed control approach is proposed for frequency control and congestion management; however, the optimal economic operation is not considered. On the other hand, [13] present a distributed controller for cost-minimizing frequency regulation with consideration of capacity constraints and tie-line congestion in bulk power systems. This distributed control assumes a base economic dispatch and minimizes the cost of deviation to solve capacity violations, considering the use of virtual phase estimators to identify limit violations.

This paper proposes a distributed inverter-control scheme for optimal dispatch of isolated microgrids considering congestion. Control rules are based on a decomposition of the optimal dispatch problem of a microgrid, and relies on local voltage and frequency measurements, as well as global congestion alerts triggered by current measurements in selected distribution lines. The contributions of this paper are as follows:

(i) A novel distributed control architecture for frequency control, congestion management, and optimal operation of the microgrid is proposed.
(ii) The proposed control strategy solves KKT conditions of a linear OPF formulation based on real system measurements, without requiring a mathematical power flow model.
(iii) We provide strong evidence via simulations that the controller is able to restore the optimal operation of the microgrid in the time-scale of the secondary frequency control. Moreover, the equivalence of the controller steady-state and KKT conditions of a linear OPF formulation is demonstrated.

This paper is organized as follows: In Section II the proposed distributed control is explained in detail. Section III presents the simulation results. Finally, conclusions are drawn in Section IV.

II. Distributed Control Strategy for Eliminating Congestion

This section presents a formulation of the network-constrained optimal dispatch problem in isolated microgrids. The formulation is then used to derive a distributed frequency and congestion controller that drives the system to a solution of the optimal dispatch problem. The proposed controller assumes the availability of current measurements from distribution lines and local DG controllers, all of which are shared through a communications network that allows bidirectional exchange of information.

A. Centralized Optimal Dispatch

Let's consider a balanced three-phase isolated microgrid, with a set of buses $\mathcal{J} = \{1, \ldots, J\}$, a set of DGs $\mathcal{N} = \{1, \ldots, N\}$ and a set of distribution lines $\mathcal{L} = \{1, \ldots, L\}$. Each bus is equipped with either a generation unit, a load, or both.

Inductive lines of reactance X_{ij} connect buses i and j. Generation units inject real power P_i to the microgrid, which is constrained within minimum and maximum limits.

The optimal dispatch problem considered in this work determines the least-cost dispatch of controllable DG units in a microgrid while maintaining line currents within limits. The formulation is based on a single-bus system representation without losses; however, line capacity limits are imposed by additional constraints on DG power injections, as follows:

$$\underset{\mathbf{P}}{\text{minimize}} \quad \sum\nolimits_{i\in\mathcal{N}} C_i(P_i) \tag{1a}$$

$$\text{subject to} \quad P_D = \sum\nolimits_{i\in\mathcal{N}} P_i \tag{1b}$$

$$I_\ell(\mathbf{P}) \le I_\ell^{\max} \;\forall\; \ell \in \mathcal{L} \tag{1c}$$

$$P_i^{\min} \le P_i \le P_i^{\max} \;\forall\; i \in \mathcal{N} \tag{1d}$$

where $\mathcal{N}$ and $\mathcal{L}$ are the sets of DGs and distribution lines in the microgrid, respectively, P_i is the real power dispatch of generator i, $C_i(P_i)$ is a convex cost function, $\mathbf{P} = \{P_i : i \in \mathcal{N}\}$, P_D is the total microgrid demand, and $I_\ell^{\max}$ is the current limit of line ℓ.

The function $I_\ell(\mathbf{P})$ represents the magnitude of the current in distribution line ℓ in terms of the real power dispatch of DGs. In general, $I_\ell(\mathbf{P})$ is a non-linear function [24], and hence the optimization problem (1) is non-convex.

By considering the following linear approximation of $I_\ell(\mathbf{P})$ at a particular operating point I_ℓ^0:

$$I_\ell(\mathbf{P}) \approx I_\ell^0 + \sum\nolimits_{i=1}^{n} P_i G_{i\ell}$$

equation (1c) can be replaced by:

$$I_\ell^0 + \sum\nolimits_{i\in\mathcal{N}} P_i G_{i\ell} \le I_\ell^{\max} \quad \forall\ \ell \in \mathcal{L}, \tag{2}$$

where $G_{i\ell}$ corresponds to the participation factor of generator i in the current of distribution line ℓ. For a particular operating point $G_{i\ell}$ includes the sign of the current; thus lower limits on line currents are not required. It is assumed that participation factors $G_{i\ell}$ can be externally provided by, for example, an online estimator. The $G_{i\ell}$ estimation methodology used in this work is described in detail in Section II-B.

The non-convex inequality constraints (1c) are replaced by (2); then, the problem (1) becomes convex. It is assumed that Slater's constraint qualification condition holds, implying strong duality, and that the problem may be studied through its Lagrange dual. The Lagrangian function of the optimal dispatch problem (1a), (1b), and (1d), using the linear approximation of functions $I_\ell(\mathbf{P})$ (2) is:

$$\begin{aligned}\mathbb{L}\left(P_i, \lambda, \gamma_\ell, \sigma_i^+, \sigma_i^-\right) = &\sum\nolimits_{i\in\mathcal{N}} C_i(P_i) + \lambda\left(P_D - \sum\nolimits_{i\in\mathcal{N}} P_i\right)\\ &+ \sum\nolimits_{\ell\in\mathcal{L}} \gamma_\ell\left(I_\ell^0 + \sum\nolimits_{i\in\mathcal{N}} P_i G_{i\ell} - I_\ell^{\max}\right)\\ &+ \sum\nolimits_{i\in\mathcal{N}} \sigma_i^+\left(P_i - P_i^{\max}\right)\\ &+ \sum\nolimits_{i\in\mathcal{N}} \sigma_i^-\left(P_i^{\min} - P_i\right)\end{aligned} \tag{3}$$

where the Lagrange multiplier λ is associated with the power balance constraint (1b), $\{\gamma_\ell\}$ with line capacity limits (2), and $\{\sigma_i^+, \sigma_i^-\}$ with the maximum and minimum power outputs of DGs in equation (1d), respectively. The KKT optimality conditions of the problem are:

Stationarity Condition:

$$\frac{\partial \mathbb{L}}{\partial P_i} = \nabla C_i(P_i) - \lambda + \sum\nolimits_{\ell\in\mathcal{L}} \gamma_\ell G_{i\ell} + \sigma_i^+ - \sigma_i^- = 0 i \in \mathcal{N} \tag{4a}$$

Complementary Slackness:

$$\gamma_\ell\left(I_\ell^0 + \sum\nolimits_{i\in\mathcal{N}} P_i G_{i\ell} - I_\ell^{\max}\right) = 0 \qquad \ell \in L \tag{4b}$$

$$\sigma_i^+\left(P_i - P_i^{\max}\right) = 0 \qquad i \in \mathcal{N} \tag{4c}$$

$$\sigma_i^-\left(P_i^{\min} - P_i\right) = 0 \qquad i \in \mathcal{N} \tag{4d}$$

Primal Feasibility:

(1b), (1d) and (2)

Dual Feasibility:

$$\gamma_\ell,\ \sigma_i^+,\ \sigma_i^- \ge 0 \qquad i \in \mathcal{N}\ \ \ell \in L \tag{4e}$$

From (4a), it follows that at the optimal point, it must be true that

$$\lambda = \nabla C_i(P_i) + \sum\nolimits_{\ell\in\mathcal{L}} \gamma_\ell G_{i\ell} + \sigma_i^+ - \sigma_i^- \quad i \in \mathcal{N} \tag{5}$$

Based on the optimality conditions of the centralized optimal dispatch problem, a new distributed control strategy is designed with the objective of providing frequency regulation, while driving the microgrid to an optimal dispatch that complies with the KKT conditions (4).

Note that the formulation of the optimization problem does not include the coupling between line-currents and reactive power injections, since it is assumed the DAPI voltage control described in [5], and implemented in our case studies, controls reactive power injections to maintain voltages in their nominal values at all nodes. Thus, this work focuses on frequency control and congestion control by means of optimally dispatching of real power of DG units.

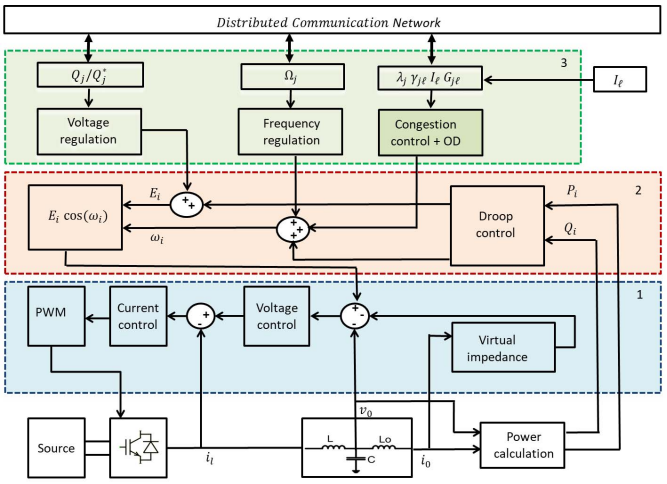

Fig. 1. Distributed control architecture for each DG.

B. Online Estimator of $G_{i\ell}$ Factors

The online estimation methodology considers an event-based update of participation factors $G_{i\ell}$, summarized as follows:

(i) Instantaneous participation factors $G_{i\ell}^*(t)$ are continuously calculated as $G_{i\ell}^*(t) = \Delta I_\ell(t)/\Delta P_i(t)$, $\forall\ell$, where $\Delta P_i(t) = P_i(t) - P_i^{ref}$ and $\Delta I_\ell(t) = I_\ell(t) - I_\ell^{ref}$. Parameters P_i^{ref} and I_ℓ^{ref} correspond to a previous operating point of the microgrid for which the current participation factors are deemed valid.

(ii) Variables $P_i(t)$ are monitored for changes beyond a pre-defined threshold with respect to P_i^{ref} (e.g., 5% changes). Let us call t^* the time for which such condition is verified.

(iii) Parameters $G_{i\ell}$ are updated after a pre-defined deadband period δ, as $G_{i\ell} = G_{i\ell}^*(t^* + \delta)$, and parameters P_i^{ref} and I_ℓ^{ref} are updated as $P_i^{ref} = P_i(t^* + \delta)$, $I_\ell^{ref} = I_\ell(t^* + \delta)$. Parameter δ is necessary to allow the instantaneous participation factors to arrive to a steady-state value after a disturbance in the system, in order to avoid unnecessary oscillations in the congestion controller. In particular, we use a value of $\delta = 0.5s$ in our case studies.

C. Distributed Control Scheme

Fig. 1 shows the architecture of local controllers of each DG that enables the distributed control strategy. Three control layers are distinguished. The first layer corresponds to the output voltage and current controls, which rely only on local measurements. The second control layer corresponds to the primary droop, which determines the reference of frequency (ω_i) and voltage (E_i), used in the first control layer. Finally, the third control layer is related to voltage and frequency

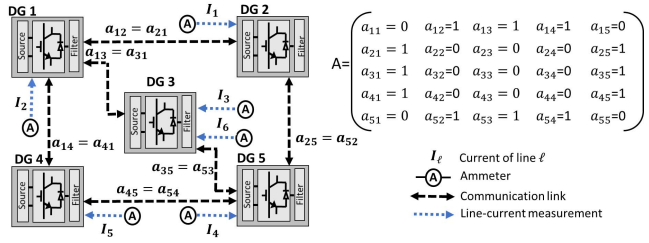

Fig. 2. Communication topology and adjacency matrix.

regulation, and the proposed congestion control. The voltage regulation control maintains the voltage at its nominal value, whereas the frequency regulation and proposed congestion control change the reference of the frequency droop controllers in order to maintain the frequency at its nominal value, remove the overloading of distribution lines, and drive the system to an optimal dispatch. In order to achieve the objectives of the third layer, local DG controllers minimize the terms of the lagrangian function in (3) associated with their local variables for given values of lagrangian multipliers. Then, by using a distributed averaging strategy, the controllers converge to unique global values of such multipliers. The exchange of information between local DG controllers occurs through the communication network shown in Fig. 1. The required communication netwok, frequency regulation control and congestion control strategies are explained in more detail in the following sections.

D. Communication Structure

A communication network is required for the implementation of the proposed distributed control scheme. The bidirectional network is modelled as an undirected graph $\mathbb{G} = (\mathcal{N}, \mathcal{E}, A)$ between the DG units $\mathcal{N} = \{1, \ldots, N\}$, where $\mathcal{E}$ is the set of communication links and A is the nonnegative $N \times N$ weighted adjacency matrix. The elements of A are $a_{ij} = a_{ji} \geq 0$, with $a_{ij} > 0$ if and only if $\{i, j\} \in \mathcal{E}$ [5], [25]. Let $x_i \in \mathbb{R}$ denote the value of some quantity of interest at bus i; in our specific context, x_i will be an internal controller variable. It is said the variables x_i achieve consensus if $x_i(t) - x_j(t) \to 0$ as $t \to \infty$. Consensus can be achieved via the following algorithm [26]:

$$\dot{x}_i = -\sum\nolimits_{j\in\mathcal{N}(i)} a_{ij}(x_i - x_j)$$

which is distributed according to the topology of the communication network.

Remark 1 (Communication Requirements): The communications network through which the DG units exchange information, defined by the adjacency matrix A (see Fig. 2), does not necessarily have the same topology as the electric network of the microgrid. In this work, in order to ensure the optimal dispatch, power sharing, and congestion management, the communications network must allow bidirectional exchange of information. Also an ideal communication (without delays) is assumed. Notice that the use of the adjacency matrix can be extended to discrete, asynchronous and synchronous communication with delays [5], [25].

E. DAPI Frequency Regulation and Active Power Sharing

The distributed-averaging proportional-integral (DAPI) approach presented in [5] is used in this work for frequency regulation. The droop frequency ω_i is defined by (6), where m_i is $P - \omega$ droop coefficient, P_i is the active power injection, and ω^* is the nominal frequency of the microgrid. The term Ω_i in (6) corresponds to the secondary control action for frequency regulation, which is obtained from (7).

$$\omega_i = \omega^* - m_i P_i + \Omega_i \tag{6}$$

$$k_i\dot{\Omega}_i = -\big(\omega_i - \omega^*\big) - \sum\nolimits_{j\in\mathcal{N}(i)} a_{ij}\big(\Omega_i - \Omega_j\big) \tag{7}$$

In (7), k_i represents the integral gain of the controller for frequency restoration, the first term on the right-hand-side corresponds to the frequency error, whereas the second term is introduced so that Ω_i converges to a unique value for all DG units, guaranteeing that all droop curves are shifted by the same amount. Terms a_{ij} represent the entries of the adjacency matrix; thus, the control action Ω_j is shared with generator i only if a_{ij} is nonzero.

F. Congestion Control and Optimal Operation

This section presents a novel distributed congestion control to eliminate overloading in distribution lines of microgrids while maintaining optimality of dispatch (8). The design is based on the convex optimization problem (1a), (1b), (1d) and (2) presented in Section II-A, and has some similarities with the controller presented in [23]; however, they are based on different design principles. Important differences between the controllers include: i) the proposed controller resolves limit violations based on current and power measurements, whereas [23] relies on a linear power flow model of the network, ii) the control actions in our controller can be directly interpreted as the dual variables of the centralized optimal dispatch problem in steady state, and iii) the congestion of lines in our controller is defined in terms of line currents instead of real power, which is more appropriate for distribution systems.

$$\omega_i = \omega^* - m_i(P_i) + \Omega_i + \rho_i \tag{8a}$$

$$k_i\dot{\Omega}_i = -\big(\omega_i - \omega^*\big) - \sum\nolimits_{j\in\mathcal{N}(i)} a_{ij}\big(\Omega_i - \Omega_j\big) \tag{8b}$$

$$k_i^1\dot{\rho}_i = -\sum\nolimits_{j\in\mathcal{N}(i)} a_{ij}\big(\lambda_i - \lambda_j\big) \tag{8c}$$

$$k_i^2\dot{\gamma}_{i\ell} = -\sum\nolimits_{j\in\mathcal{N}(i)} a_{ij}\big(\gamma_{i\ell} - \gamma_{j\ell}\big) + \mu_i^1 \max\left\{I_\ell + \frac{1}{\mu_i^1}k_i^3\gamma_{i\ell} - I_\ell^{\max}, 0\right\} - k_i^3\gamma_{i\ell} \tag{8d}$$

$$k_i^4\dot{\sigma}_i^+ = \mu_i^2 \max\left\{P_i + \frac{1}{\mu_i^2}k_i^5\sigma_i^+ - P_i^{\max}, 0\right\} - k_i^5\sigma_i^+ \tag{8e}$$

$$k_i^6\dot{\sigma}_i^- = \mu_i^3 \max\left\{P_i^{\min} + \frac{1}{\mu_i^3}k_i^7\sigma_i^- - P_i, 0\right\} - k_i^7\sigma_i^- \tag{8f}$$

$$\lambda_i = \nabla C_i(P_i) + \sum\nolimits_{\ell\in\mathcal{L}} \gamma_{i\ell}G_{i\ell} + \sigma_i^+ - \sigma_i^- \tag{9}$$

The proposed controller aims at driving the system to an optimal dispatch that complies with the KKT conditions of

the problem. For this purpose, equation (6) is modified as (8a), where the additional term ρ_i is a secondary control action to drive the units to their optimal dispatch level considering congestion in the lines, and k_i^1 is a positive gain of the controller. In particular, control actions ρ_i will introduce a perturbation to the frequency droop controller in (8a) that changes the dispatch of DGs until all units reach the same value of λ, which corresponds to the (unique) dual variable associated with the demand-supply balance equation of the microgrid's optimal dispatch problem, (1b). The condition of $\lambda_i = \lambda_j = \lambda$ in steady-state is enforced by equation (8c).

As in (2), $G_{i\ell}$ represents the participation factor of unit i in the current of line ℓ, and it is obtained from an external online estimator.

Based on equation (5), the λ_i of each DG that complies with the stationarity condition can be calculated from (9). Variable $\gamma_{i\ell}$ is a distributed congestion control action; $\gamma_{i\ell}$ in equilibrium corresponds to the dual variable γ_ℓ in (4b). Finally, σ_i^+ and σ_i^- are local control actions to keep the active power dispatch of DG units within limits, which in equilibrium correspond to the dual variables associated with maximum and minimum active power limits, respectively.

The control action $\gamma_{i\ell}$ is obtained from equation (8d), where the first term on the right-hand-side introduces a perturbation whenever there is a mismatch between the $\gamma_{i\ell}$'s observed by neighbouring DGs. This is necessary in order to obtain unique γ_ℓ actions in steady state, which can then be interpreted as dual variables of line-current limit equations (2). The second and third terms induce an increase in the value of $\gamma_{i\ell}$ in case of overloading of line ℓ, and a decrease down to zero when the overloading is (strictly) resolved. This is consistent with the fact that, if line ℓ is overloaded, the value of γ_ℓ is being underestimated by the controller; hence, it must be increased. Similarly, if the line-current limit is non-binding, the value of γ_ℓ must decrease down to zero. Finally, k_i^2, k_i^3, and μ_i^1 are positive gains of the controller. It is assumed throughout the paper that $k_i^3/\mu_i^1 = \kappa > 0$ for all $i \in \mathcal{N}$.

Likewise, equations (8e) and (8f) induce increases in the values of σ_i^+ and σ_i^- whenever unit i goes beyond its maximum or minimum active power dispatch levels, respectively. Also, control actions σ_i^+ and σ_i^- are driven down to zero by the second term of the controller if the active power dispatch of unit i is strictly within limits, where k_i^4, k_i^5, k_i^6, k_i^7, μ_i^2 and μ_i^3 are positive gains of the controllers.

The design and proper operation of the proposed distributed controller relies on the following assumptions:

(i) Each DG in the microgrid is able to communicate Ω_i, λ_i, $\gamma_{i\ell}$, I_ℓ to neighboring DGs through a connected and bidirectional communication network.
(ii) Each DG has information of $\gamma_{i\ell}$ for all distribution lines of the microgrid, and each line subject to congestion has at least one DG with non-zero participation factor associated.
(iii) Current measurements of all distribution lines are available to the local controllers of all DGs in the microgrid.
(iv) Participation factors $G_{i\ell}$ are calculated with reasonable accuracy by an external online estimator and are available to each DG.

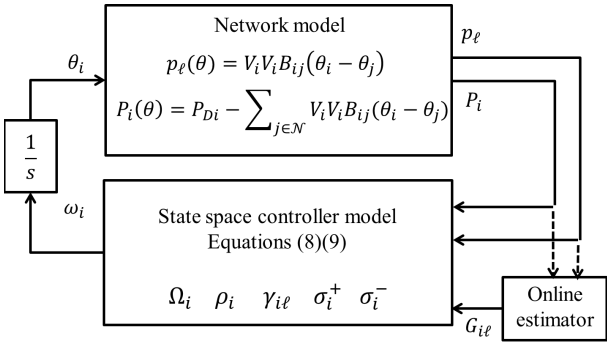

Fig. 3. Close-loop microgrid system.

(v) Reactive power is only used for voltage control, and it is not available for solving overloading problems.
(vi) There is no conflict between control actions of congestion controllers of the different lines.

G. Closed-Loop Microgrid System

Fig. 3 shows the closed-loop microgrid system. The network model is defined by (10), where $p_\ell(\theta)$ in (10a) is the power flow from the line ℓ, B_{ij} is the line susceptance, and V_i and V_j are the voltages at i and j nodes. In (10b) the active power in the DG i is defined, where P_{Di} is the demand at the node i.

$$p_\ell(\theta) = V_i V_j B_{ij}(\theta_i - \theta_j) \qquad \ell = \{i, j\} \quad (10a)$$

$$P_i(\theta) = P_{Di} - \sum\nolimits_{j\in\mathcal{N}} V_i V_j B_{ij}(\theta_i - \theta_j) \qquad i \in \mathcal{N} \quad (10b)$$

Using also the proposed distributed control (8) and (9), the closed-loop microgrid system is given by the following equations (11)

$$\dot{\theta}_i = \omega^* - \omega_i \quad (11a)$$

$$\dot{\theta}_i = -m_i(P_i) + \Omega_i + \rho_i \quad (11b)$$

$$k_i \dot{\Omega}_i = m_i(P_i) - \Omega_i - \rho_i - \sum\nolimits_{j\in\mathcal{N}(i)} a_{ij}(\Omega_i - \Omega_j) \quad (11c)$$

$$k_i^1 \dot{\rho}_i = -\sum\nolimits_{j\in\mathcal{N}(i)} \left(\nabla C_i(P_i) + \sum\nolimits_{\ell\in\mathcal{L}} \gamma_{i\ell} G_{i\ell} + \sigma_i^+ - \sigma_i^-\right) - \left(\nabla C_j(P_j) + \sum\nolimits_{\ell\in\mathcal{L}} \gamma_{j\ell} G_{j\ell} + \sigma_j^+ - \sigma_j^-\right) \quad (11d)$$

$$k_i^2 \dot{\gamma}_{i\ell} = -\sum\nolimits_{j\in\mathcal{N}(i)} a_{ij}(\gamma_{i\ell} - \gamma_{j\ell}) + \mu_i^1 \max\left\{I_\ell + \frac{1}{\mu_i^1} k_i^3 \gamma_{i\ell} - I_\ell^{\max}, 0\right\} - k_i^3 \gamma_{i\ell} \quad (11e)$$

$$k_i^4 \dot{\sigma}_i^+ = \mu_i^2 \max\left\{P_i + \frac{1}{\mu_i^2} k_i^5 \sigma_i^+ - P_i^{\max}, 0\right\} - k_i^5 \sigma_i^+ \quad (11f)$$

$$k_i^6 \dot{\sigma}_i^- = \mu_i^3 \max\left\{P_i^{\min} + \frac{1}{\mu_i^3} k_i^7 \sigma_i^- - P_i, 0\right\} - k_i^7 \sigma_i^-. \quad (11g)$$

H. Distributed Congestion Control Optimality

This subsection discusses the optimality of the stationary points of the proposed distributed controller.

The optimum solution of the optimization problem described by (1a), (1b), (1d), and (2), must comply with the

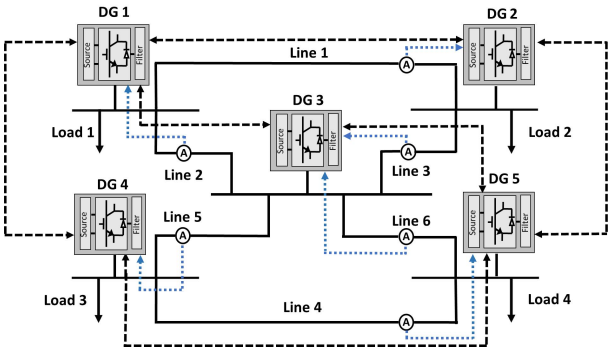

Fig. 4. Microgrid study case.

KKT conditions. Thus, in the following, we show that an equilibrium point of the closed-loop system (11) also verifies the KKT conditions in (4a)-(4e).

Theorem 1 (Distributed Optimal Dispatch): Consider the optimal dispatch problem (1a), (1b), (1d), and (2), and the closed-loop microgrid system (11). Assume that the dispatch problem has a strictly feasible point. Let $(\theta_i^*, \Omega_i^*, \rho_i^*, \gamma_{i\ell}^*, (\sigma_i^+)^*, (\sigma_i^-)^*)$ be an equilibrium point of the closed-loop microgrid, and let

$$P_i^* := P_{Di} - \sum\nolimits_{j\in\mathcal{N}(i)} V_i V_j B_{ij}\left(\theta_i^* - \theta_j^*\right), \qquad i \in \mathcal{N}$$
$$\lambda_i^* := \nabla C_i\left(P_i^*\right) + \sum\nolimits_{\ell\in\mathcal{L}} \gamma_{i\ell}^* G_{i\ell} + \left(\sigma_i^+\right)^* - \left(\sigma_i^-\right)^*$$

be the real power injections of each DG unit, and their lagrangian multipliers associated with the demand-supply balance equation. The following statements hold:

(i) for each $\ell \in \{1, \ldots, L\}$, there is a constant $\gamma_\ell^* \geq 0$ such that

$$\gamma_{i\ell}^* = \gamma_\ell^* \quad \text{for all} \quad i \in \mathcal{N};$$

(ii) there is a constant λ^* such that

$$\lambda_i = \lambda^* \quad \text{for all} \quad i \in \mathcal{N};$$

(iii) $(P_i^*, \lambda^*, \gamma_\ell^*, (\sigma_i^+)^*, (\sigma_i^-)^*)$ is an optimal point of the optimization problem (1a), (1b), (1d), and (2).

The proof of Theorem 1 is presented in the Appendix of the paper.

III. Simulation Results

A. Microgrid Configuration

In order to validate the proposed distributed control strategy, its performance is assessed in a case study using the microgrid configuration shown in Fig. 4. The microgrid is composed of five DG units, six distribution lines and four distributed loads. The characteristics of DG units and network parameters are given in Table I and Table II, respectively. The generation cost functions of DG unit are assumed quadratic ($C_i = \alpha_i P_i^2 + \vartheta_i P_i + \psi_i$), with parameters shown in Table III [27]. The communications network is represented by dashed lines in Fig. 4. The control scheme shown in Fig. 1 is implemented in each DG unit, together with the proposed distributed control described by equations (8) and (9).

TABLE I
DG Characteristics

Parameter	Symbol	DG1-DG5
Maximum Active Power	P_i^{max}	2kW
Minimum Active Power	P_i^{min}	0kW
P-W Droop Coefficient	m_i	0.0025
Q-E Droop Coefficient	n_i	0.0015
Frequency Control Gain	k_i	0.5
Congestion Control Gain 1	k_i^1	0.5
Congestion Control Gain 2	k_i^2	0.25
Congestion Control Gain 4	k_i^4	0.1
Congestion Control Gain 6	k_i^6	0.1
Congestion Control Gain 7	$k_i^3/\mu_i^1 = \kappa$	10
Voltage Control Gain	$\mathbf{k_i}$	1

TABLE II
Microgrid Parameters

Parameter	Symbol	Value
Nominal Frequency	$\omega^*/2\pi$	50 Hz
Nominal Voltage	E^*	230 Vrms
Filter Capacitance	C	25μF
Filter Inductance	L_f	1.8mH
Output Impedance	L_o	1.8mH
Line Impedance 1	R,L	0.7Ω, 1.9mH
Line Impedance 2	R,L	0.7Ω, 1.9mH
Line Impedance 3	R,L	0.7Ω, 1.9mH
Line Impedance 4	R,L	0.7Ω, 1.9mH
Line Impedance 5	R,L	0.7Ω, 1.9mH
Line Impedance 6	R,L	0.7Ω, 1.9mH

TABLE III
DG Cost Parameters

Parameter	DG1	DG2	DG3	DG4	DG5
α_i [\$/kW^2]	0.264	0.444	0.4	0.5	0.25
ϑ_i [\$/kW]	0.067	0.111	0.1	0.125	0.063
ϕ_i [\$]	0	0	0	0	0

The simulation was performed using the software PLECS [28], considering current measurements from each line, and local measurements of frequency, real power injection, output current, and voltage.

For voltage regulation purpose, DAPI voltage-regulation and reactive-power-sharing controllers are implemented based on [5]. The droop voltage E_i is defined by (12), where n_i represents the Q-E droop coefficient, E^* is the nominal voltage of the microgrid, Q_i is the reactive power injection, and e_i is the control action for voltage regulation, obtained from equation (13); e_i establishes a trade-off between voltage regulation and reactive power sharing, where Q_i^* is the reactive power rating of unit i. The consensus approach is used in order to achieve proportional reactive power sharing, where the normalized reactive power injection $\frac{Q_j}{Q_j^*}$ of each DG is transmitted through the communications network shown in Fig. 2.

The terms β_i and k_i are positive gains, and b_{ij} is an element of the adjacency matrix of the bidirectional communications network.

$$E_i = E^* - n_i Q_i + e_i \tag{12}$$
$$\mathbf{k_i}\dot{e}_i = -\beta_i\left(E_i - E^*\right) - \sum\nolimits_{j\in\mathcal{N}(i)} b_{ij}\left(\frac{Q_i}{Q_i^*} - \frac{Q_j}{Q_j^*}\right). \tag{13}$$

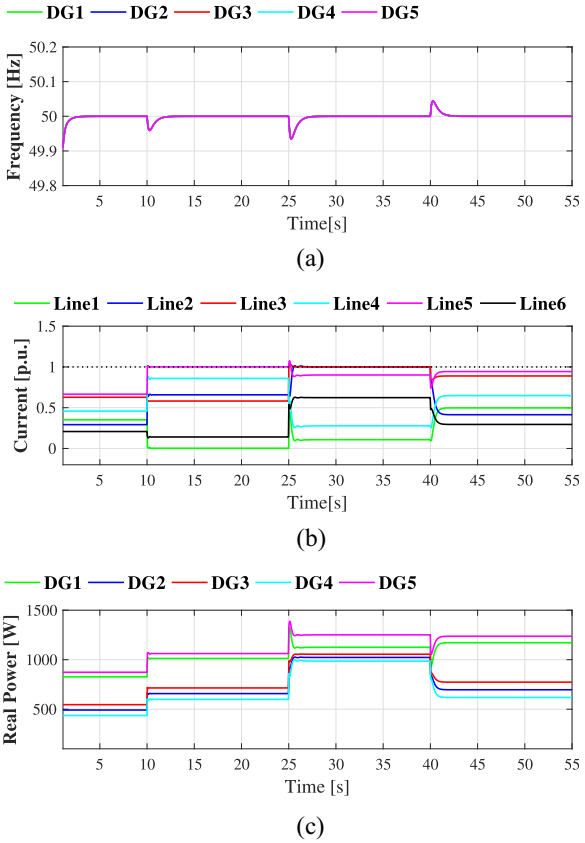

Fig. 5. Distributed congestion control response (a) Frequency at each DG, (b) Current in the lines, (c) Real power injection for each DG.

B. Simulation Setup

Simulations of the dynamic performance of the controllers were carried out using a time-frame of 55 seconds. At 10 seconds, a 34% incremental step-change is applied to loads 1 and 3, and a 5% incremental step-change is applied to loads 2 and 4, producing the congestion of line 5. At 25 seconds, another 12% incremental step-change is applied to loads 1 and 3, and a 39% incremental step-change is applied to loads 2 and 4, yielding an overload of lines 2 and 3 of the microgrid. Finally, at 40 seconds, an 18% decremental step-change is applied to all loads.

The controller gains were tuned using a heuristic approach, where a first approximation of the gains was obtained using the root locus method applied to a condition where all the controllers are active (i.e., all the *max* operators take the value of the first argument). Then, several simulations were carried out for different operating points in order to fine-tune the gains, with satisfactory results. A more precise tuning of the controller could be performed using meta-heuristic optimization techniques; however, this is not addressed in the present work.

C. Simulation Results

In this section, the dynamic performance of the proposed controller (8), (9) is illustrated and discussed. It can be observed from Fig. 5a and Fig. 5b that the controller is able to successfully restore frequency and resolve congestion after each load perturbation. In specific, Fig. 5a shows how the controller is able to restore the frequency of all DG units to their nominal value, after a transient of limited excursion. Likewise, Fig. 5b illustrates that thanks to the correct performance of the controller (8c)-(8f), (9), the congestion is quickly eliminated by driving line currents within limits. Fig. 5b shows that before the first step-change in load all line currents are below their maximum limit, whereas Fig. 5c shows that the load's real power is shared unevenly among the 5 DG units, due to their different cost functions. At 10 seconds, the first step-change occurs and line 5 becomes overloaded; however, the distributed congestion controller removes the overloading in less than 3 seconds, which is fast enough to avoid the activation of thermal protections in distribution lines. At 25 seconds, a second step-change in load is applied, resulting in an overloading of lines 2 and 3. Once again, the congestion control is able to resolve the congestion within a few seconds, as shown in Fig. 5b (from 25 to 45 seconds).

The real power injected by each DG is shown in Fig. 5c. When the congestion control action is zero (from 0 to 10 seconds and 40 to 55 seconds), the load's real power is shared among the DG units according to their operating cost (Table III). However, when a control action is required to resolve a congestion (from 10 to 40 seconds), the real power injections of DG units are redistributed in order to remove the line overloading based on their different cost functions and participation factors.

The frequency restoration is driven by the control actions Ω_i in each DG unit, which are shown in Fig. 6a. It can be observed that the actions converge to a unique value for all units that restores nominal frequency. Figures 6b, 6c, and 6d show the control actions $\gamma_{i\ell}$ used to remove the congestion in each line, respectively. On the other hand, Fig. 6d shows how γ_{i5} are nonzero in the 10 to 25 seconds time-window in order to resolve the congestion in line 5. Likewise, in Fig. 6b and Fig. 6c the 25 to 40 seconds time-window, both γ_{i2} and γ_{i3} control actions are required.

Fig. 7 shows the λ_i of each DG unit. It can be observed that, in steady-state the values of λ_i converge to a unique value for all units, which then corresponds to the dual variable associated with the demand-supply balance equation in the centralized optimal dispatch problem.

In order to analyze the performance of the controller against the sudden loss of a DG unit, we simulate a 34% incremental step-change in loads 1 and 3, and a 5% incremental step-change in loads 2 and 4 at 10 seconds, and the sudden loss of unit DG2 at 20 seconds, with both frequency regulation and congestion controllers activated. The simulation results are shown in Fig. 8. Fig. 8a shows that after the disconnection of DG2, frequency is restored to its nominal value within 2-3 seconds; moreover, Fig. 8b shows that the congestion in line 4 produced by the the disconnection of DG2 is eliminated by the congestion controller (from 20 to 40 seconds). Fig. 8c shows that at 20 seconds the real power of unit DG2 is drops to zero, and the remaining units increase their real power injections in order to satisfy the microgrid's demand, which remains unchanged, and considering the operating cost.

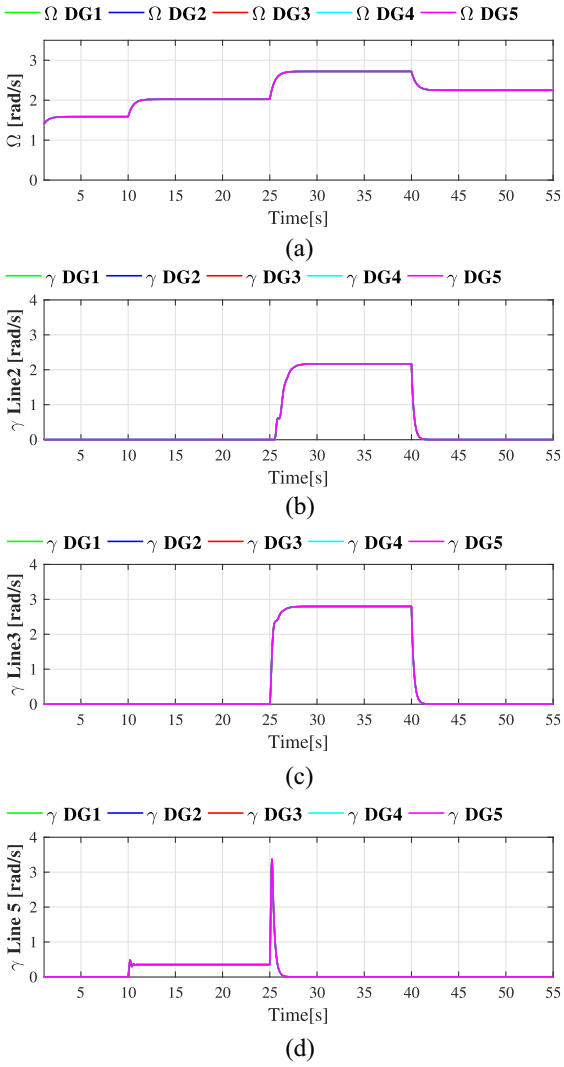

Fig. 6. (a) Control action for frequency regulation, (b) Congestion control action for line 2, (c) Congestion control action for line 3, (d) Congestion control action for line 5.

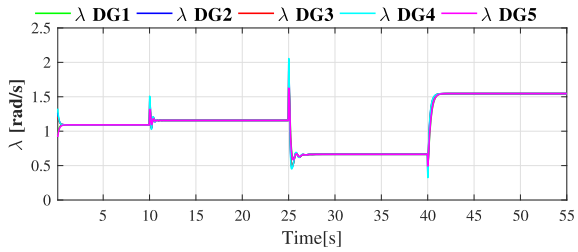

Fig. 7. Lagrange multiplier λ.

In order to analyze the performance of the controller against communication link failures we simulate a 34% incremental step-change in loads 1 and 3, and a 5% incremental step-change in loads 2 and 4 at 10 seconds, followed by the simultaneous failure of the communication links between units DG1 and DG2, and units DG3 and DG5 at 20 seconds, illustrated in Fig. 9. Finally, a decremental step-change in loads is applied at 30 seconds to restore the initial loading of the microgrid. The simulation results are shown in Fig. 10. It is

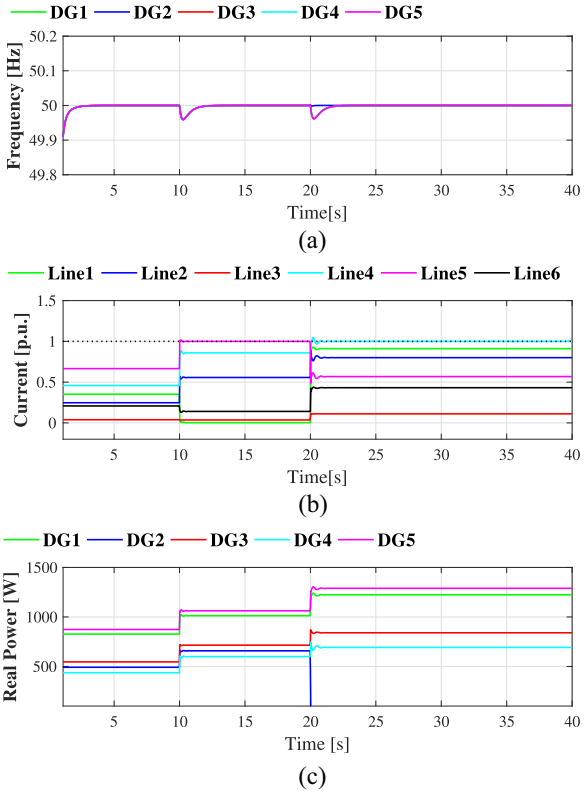

Fig. 8. Distributed congestion control response test by disconnecting DG2 (a) Frequency in each DG, (b) Current from the lines, (c) Real power injections for each DG.

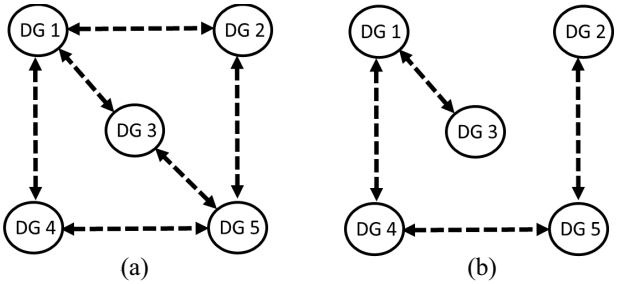

Fig. 9. Microgrid communication topology (a) Original topology, (b) Topology with communication links failure.

observed that the proposed controller does not suffer noticeable deterioration in its performance against the loss of the communication links. Noteworthy, this results assume that the units have a dynamic adjacency matrix, which is instantly updated upon loss of communication links.

In order to analyze the performance of the controller against communication delays, we introduce constant delays τ_i in the consensus terms of the controller, as shown in equations (14). We simulate a 34% incremental step-change in loads 1 and 3, and a 5% incremental step-change in loads 2 and 4 at 30 seconds, and the performance of the controller is analyzed for two cases: a) small time-delays ($\tau_i = 0.05s$), and b) large time-delays ($\tau_i = 1s$).

$$k_i \dot{\Omega}_i = -\left(\omega_i - \omega^*\right) - \sum\nolimits_{j \in \mathcal{N}(i)} a_{ij}\left(\Omega_i - \Omega_j(t - \tau_i)\right) \quad (14a)$$

$$k_i^1 \dot{\rho}_i = -\sum\nolimits_{j \in \mathcal{N}(i)} a_{ij}\left(\lambda_i - \lambda_j(t - \tau_i)\right) \quad (14b)$$

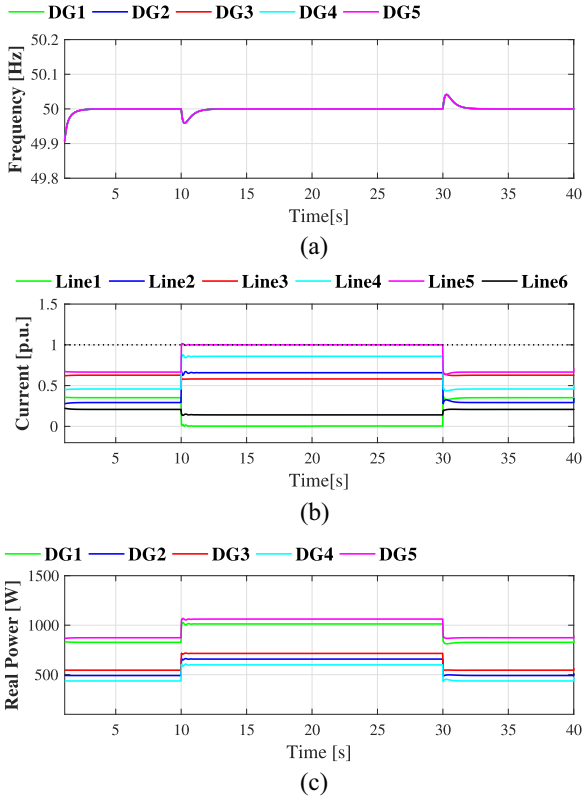

Fig. 10. Distributed congestion control response test by communication link failure between (DG1 and DG2), and (DG3 and DG5) (a) Frequency in each DG, (b) Current from the lines, (c) Real power injections for each DG.

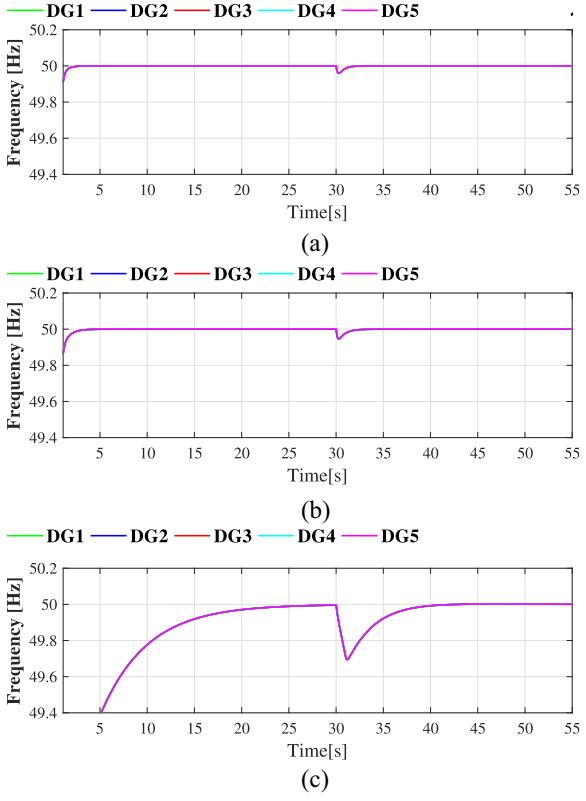

Fig. 11. Frequency response test with communication delay (a) Without time-delay, (b) With small time-delays $\tau_i = 0.05s$, (c) With large time-delays $\tau_i = 1s$.

$$k_i^2 \dot{\gamma}_{i\ell} = -\sum\nolimits_{j\in\mathcal{N}(i)} a_{ij}\big(\gamma_{i\ell} - \gamma_{j\ell}(t-\tau_i)\big) + \mu_i^1 \max\left\{ I_\ell(t-\tau_i) + \frac{1}{\mu_i^1} k_i^3 \gamma_{i\ell} - I_\ell^{\max}, 0 \right\} - k_i^3 \gamma_{i\ell} \tag{14c}$$

Figures 11a, 11b and 11c show the frequency of each DG for the cases of no communication delays (i.e., $\tau_i = 0s$), small time-delays ($\tau_i = 0.05s$), and large time-delays ($\tau_i = 1s$), respectively. It is observed that the performance of the controller with small time-delays is very similar to the case with no delays, where the controller is able to restore frequency in the microgrid within 2 seconds of the perturbation; however, in the case of large time-delays the restoration of frequency is achieved in a much larger time, of nearly 15 seconds after the load perturbation. Fig. 12 shows response of the distributed congestion control in terms of line currents, for the same 3 cases of time-delay. It is observed that the only line that faces congestion is line 5, and the congestion is resolved in all the cases; however, the convergence rate of the currents in the case of large time-delays shown in Fig. 12c is noticeably slower than the other 2 cases.

Finally, the impact of estimation errors in $G_{i\ell}$ factors is analyzed for different levels of error: i) 25% over-estimation in each $G_{i\ell}$, ii) 25% under-estimation in each $G_{i\ell}$, and iii) randomly assigned estimation error between -25% and 25% to each factor. The analysis shows that the largest deviation from optimality is obtained in the case of a 25% over-estimation of the factors, where the dispatch deviates a 0.079% from the optimal operation (without estimation errors), which represents a 5.7% of the incremental cost incurred to resolve congestion. Nevertheless, the congestion is resolved regardless of the estimation errors.

D. Eigenvalue Analysis

Using the proposed distributed congestion control, a linearized model of the closed-loop system (11) is derived. The operating point used for the linearization is obtained from a case study where two lines become congested; specifically lines 2 and 3.

Fig. 13 shows the eigenvalues obtained for the aforementioned operating point, and also illustrates the eigenvalue trajectories for increments in the gains k_i in (8b), k_i^1 in (8c), and k_i^2 in (8d). It is observed that the system is stable for the nominal values of the gains, which are presented in Table I. Critical values of the gains k_i, k_i^1 and k_i^2 were identified in order to obtain stable limits for the controller gains.

This work does not include any theoretical stability analysis of the closed-loop system; nevertheless, formal linearization provides some qualitative insights into the system behavior.

Given the nonlinearity of the closed-loop system introduced by the *max* functions, the proposed controller necessitates a Lyapunov-based stability analysis. This could be performed using the theory of integral quadratic constraints [29], [30]; however, such analysis is outside the scope of this work.

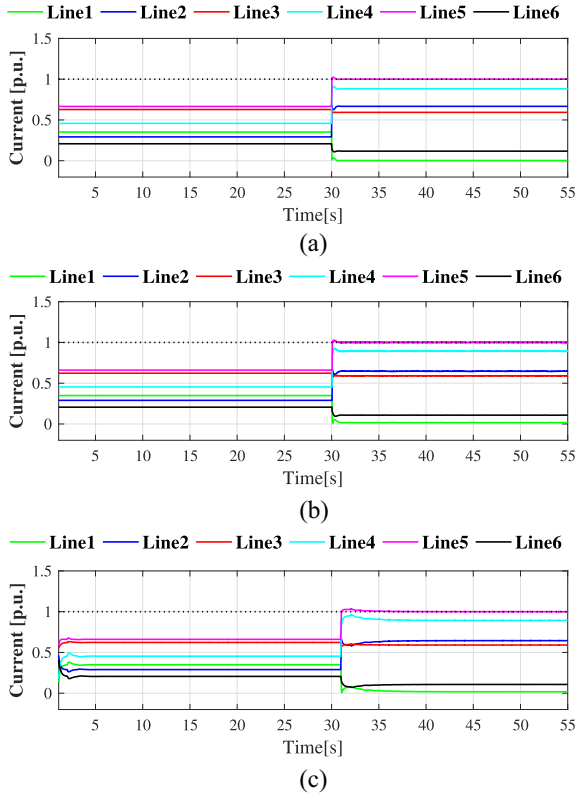

Fig. 12. Distributed congestion control response test with communication delay (a) Without time-delay, (b) With small-delays $\tau_i = 0.05s$, (c) With large-delays $\tau_i = 1s$.

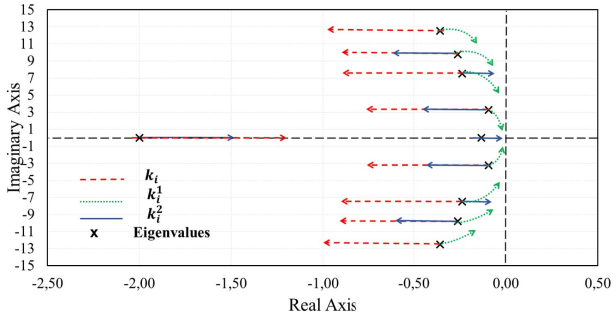

Fig. 13. Eigenvalue traces of closed-loop system (11) as controller gains are varied. (Arrows indicate the direction of increasing gain. Black crosses indicate eigenvalues for the nominal gain of (8) in the microgrid study case (Fig. 4). The most important eigenvalues have been considered.)

IV. Conclusion

This paper presented a novel distributed control strategy for frequency control, optimal operation, and congestion management of isolated microgrids. The proposed controller is capable of driving the microgrid to its optimal operation while considering output limits of DGs and thermal limits of distribution lines by using real-time measurements. The equivalence between the closed-loop steady-state conditions of the controller and the KKT conditions of a linear OPF formulation is mathematically demonstrated in the paper. The capabilities and good dynamic performance of the controller are shown and discussed using several simulations. The economic performance of the controller relies on the availability of participation factors of each DG in the current of distribution lines. The more accurate estimation of such participation factors, as well as a theoretical stability analysis of the controller will be further studied in future research. Also, future research will consider the integration of distributed voltage/reactive power control in the proposed strategy. Finally, interesting extensions of this work include the application of the proposed controller to the sharing of power imbalance and harmonics, among others.

Appendix
Proof of Theorem 1

Theorem 1 states that any equilibrium point of the closed loop system under the proposed controller is also a KKT point. We proceed by showing that any equilibrium of the closed-loop microgrid yields a solution of the KKT condition.

Stationarity Condition: We begin with (8c). Since the communication graph $\mathbb{G}$ is connected, it follows from (8c) that $\lambda_i = \lambda_j = \lambda$ for some constant λ for all i, j [26]. Equation (9) then immediately yields the KKT stationarity condition (5).

Primal Feasibility of Power Balance (1b): Equation (1b) corresponds to physical constraints of energy balance that is always satisfied in the system. From equation (11) of the closed-loop microgrid system, it is directly deductible (11a) that at equilibrium, $\omega_i = \omega^*$, this equality is satisfied when the power balance is achieved.

Complementary Slackness of DG Active Power Limits: The equations (8e) and (8f) in equilibrium yield

$$0 = \mu_i^2 \cdot \max\left\{P_i + \tfrac{1}{\mu_i^2} k_i^5 \sigma_i^+ - P_i^{\max}, 0\right\} - k_i^5 \sigma_i^+ \quad (15a)$$

$$0 = \mu_i^3 \cdot \max\left\{P_i^{\min} + \tfrac{1}{\mu_i^3} k_i^7 \sigma_i^+ - P_i, 0\right\} - k_i^7 \sigma_i^- \quad (15b)$$

for all $i \in \{1, \ldots, n\}$. We will prove that complementarity condition (4c) holds in equilibrium, using equation (15a). In light of (15a), the set of buses can be partitioned into two disjoint sets $U, V \subset \{1, \ldots, n\}$ such that

$$P_i + \frac{1}{\mu_i^2} k_i^5 \sigma_i^+ - P_i^{\max} \le 0, \qquad i \in U, \quad (16a)$$

$$P_i + \frac{1}{\mu_i^2} k_i^5 \sigma_i^+ - P_i^{\max} > 0, \qquad i \in V. \quad (16b)$$

Then equation (15a) can be reduced to

$$0 = -k_i^5 \sigma_i^+, \qquad i \in U,$$
$$0 = \mu_i^2 \left(P_i - P_i^{\max}\right), \qquad i \in V,$$

from which we conclude that $\sigma_i^+ = 0$ for all $i \in U$ and $P_i = P_i^{\max}$ for all $i \in V$. In either case, we conclude that $\sigma_i^+ (P_i - P_i^{\max}) = 0$. For $i \in U$, substitution of $\sigma_i^+ = 0$ into (16a) immediately shows that $P_i \le P_i^{\max}$ and for $i \in V$, substitution of $P_i = P_i^{\max}$ into (16b) implies that $\sigma_i^+ > 0$. We conclude that the complementary slackness condition (4c) holds, that the upper bound in (1d) is primal feasible, and that the multipliers σ_i^+ are dual feasible. Analogous arguments using (15b) show complementary slackness for σ_i^-, primal

feasibility of the lower bound in (1d), and dual feasibility of σ_i^-.

Complementarity Condition of Line Current Limits: The equation (8d) at equilibrium yields

$$0 = -\sum_{j\in\mathcal{N}(i)} a_{ij}\big(\gamma_{i\ell} - \gamma_{j\ell}\big) + \mu_i^1 \max\left\{I_\ell + \frac{1}{\mu_i^1}k_i^3\gamma_{i\ell} - I_\ell^{\max}, 0\right\} - k_i^3\gamma_{i\ell} \quad (17)$$

for all $\ell \in \{1,\dots,L\}$. We will show that the complementarity condition (4b) holds. For each line ℓ, we partition the set of DGs into two disjoint subsets $R, S \subset \{1,\dots,n\}$

$$I_\ell + \frac{1}{\mu_i^1}k_i^3\gamma_{i\ell} - I_\ell^{\max} \le 0, \quad i \in R, \quad (18a)$$

$$I_\ell + \frac{1}{\mu_i^1}k_i^3\gamma_{i\ell} - I_\ell^{\max} > 0, \quad i \in S. \quad (18b)$$

With these definitions, equation (17) reduces to

$$\sum_{j\in\mathcal{N}(i)} a_{ij}\big(\gamma_{i\ell} - \gamma_{j\ell}\big) = -k_i^3\gamma_{i\ell}, \quad i \in R, \quad (19a)$$

$$\sum_{j\in\mathcal{N}(i)} a_{ij}\big(\gamma_{i\ell} - \gamma_{j\ell}\big) = \mu_i^1\big(I_\ell - I_\ell^{\max}\big), \quad i \in S. \quad (19b)$$

The rest of the demonstration is separated in 3 cases:

- *Case I:* $S = \emptyset$ (i.e., $i \in R,\ \forall i$)
- *Case II:* $R = \emptyset$ (i.e., $i \in S,\ \forall i$)
- *Case III:* Both R and S are non-empty.

Case I: When S is empty, it follows from (19a) that

$$0 = -\sum_{j\in\mathcal{N}(i)} a_{ij}\big(\gamma_{i\ell} - \gamma_{j\ell}\big) - k_i^3\gamma_{i\ell}$$

for all $i \in \{1,\dots,n\}$. Letting $\boldsymbol{\gamma}_\ell = (\gamma_{1\ell}, \gamma_{2\ell}, \dots, \gamma_{n\ell})^\mathsf{T}$, this equation may be written in matrix form as $M\boldsymbol{\gamma}_\ell = 0$, where

$$M_{ij} = \begin{cases} -a_{ij} & \text{if} \quad i \neq j \\ \sum_{j\in\mathcal{N}(i)} a_{ij} + k_i^3 & \text{if} \quad i = j \end{cases}$$

Since $k_i^3 > 0$ for all $i \in \{1,\dots,n\}$, the symmetric matrix M has strictly positive diagonal entries and is strictly diagonally dominant; it is therefore positive definite, and we conclude that $\boldsymbol{\gamma}_\ell = 0$. We may therefore take $\gamma_\ell^* = 0$ in statement (i) of the Theorem. From (18a) then, we conclude that $I_\ell - I_\ell^{\max} \le 0$. Therefore, the primal feasibility condition (2) is satisfied, the complementary slackness condition (4b) is satisfied, and the multipliers are dual feasible.

Case II: When the set R is empty, it follows from (19b) that

$$\sum_{j\in\mathcal{N}(i)} a_{ij}(\gamma_{i\ell} - \gamma_{j\ell}) = \mu_i^1(I_\ell - I_\ell^{\max}),$$

for all $i \in \{1,\dots,n\}$. Summing all these equations, we obtain

$$\sum_{i\in\mathcal{N}}\sum_{j\in\mathcal{N}(i)} a_{ij}\big(\gamma_{i\ell} - \gamma_{j\ell}\big) = \sum_{i\in\mathcal{N}(i)} \mu_i^1\big(I_\ell - I_\ell^{\max}\big)\ \forall i, \ell$$

Since the communication graph $\mathbb{G}$ is undirected, the sum on the left is zero and we find that $\sum_{i=1}^n \mu_i^1(I_\ell - I_\ell^{max})$, which implies that $I_\ell = I_\ell^{\max}$. Substituting $I_\ell = I_\ell^{\max}$ into (18b), we find that $\gamma_{i\ell} > 0$. Substituting $I_\ell = I_\ell^{\max}$ into (19b), we find that

$$\sum_{j\in\mathcal{N}(i)} a_{ij}(\gamma_{i\ell} - \gamma_{j\ell}) = 0.$$

Since the communication graph $\mathbb{G}$ is connected, this equation holds if and only if $\gamma_{i\ell} = \gamma_{j\ell}$ for all $i, j \in \{1,\dots,n\}$.

We may therefore take $\gamma_\ell^* = \gamma_{n\ell} > 0$ in statement (i) of the theorem. We conclude that the primal feasibility condition (2) is satisfied, the complementary slackness condition (4b) is satisfied, and the multipliers γ_ℓ^* are dual feasible.

Case III: Now assume both sets S and R are non-empty. Assume first that the line ℓ is *not* congested, meaning that $I_\ell - I_\ell^{\max} \le 0$. From (18a)–(18b) it holds that

$$\big(I_\ell - I_\ell^{\max}\big) \le -\frac{1}{\mu_i^1}k_i^3\gamma_{i\ell}, \qquad i \in R,$$

$$\big(I_\ell - I_\ell^{\max}\big) > -\frac{1}{\mu_i^1}k_i^3\gamma_{i\ell}, \qquad i \in S.$$

Assuming that $k_i^3/\mu_i^1 = \kappa > 0$ for all $i \in \{1,\dots,n\}$, the above inequalities immediately imply that

$$\gamma_{i\ell} > \gamma_{j\ell}, \qquad i \in S, \quad j \in R. \quad (20)$$

Equation (19b) implies that

$$\sum_{j\in\mathcal{N}(i)} a_{ij}(\gamma_{i\ell} - \gamma_{j\ell}) \le 0, \quad i \in S.$$

Since $a_{ij} > 0$ for $j \in \mathcal{N}(i)$, this inequality implies that

$$\text{for all } i \in S \text{ there exists } j \in \mathcal{N}(i) \text{ s.t. } \gamma_{j\ell} \ge \gamma_{i\ell}. \quad (21)$$

Now let $\overline{\gamma}_S = \max_{i\in S}\gamma_{i\ell}$ and let $\mathcal{I}^* \subseteq S$ be the set of indices for which the maximum is achieved. We claim that there exists an $i^* \in \mathcal{I}^*$ such that i^* has a neighbour in the set R. To see that this is true, suppose that there was no such neighbour, which means that $\mathcal{N}(i^*) \subset S$ for all $i^* \in \mathcal{I}^*$. Then (21) implies that $\gamma_{j\ell} = \overline{\gamma}_S$ for all $j \in \mathcal{N}(i^*)$, and therefore that $\mathcal{N}(i^*) \subset \mathcal{I}^*$. Since the graph $\mathbb{G}$ is connected and R is non-empty, this argument can be repeated a finite number of times until we find an index $i^* \in \mathcal{I}^*$ with a neighbour in R. For this index, (21) implies that there exists a $j \in \mathcal{N}(i^*) \cap R$ such that $\gamma_{j\ell} \ge \overline{\gamma}_S$. However, this directly contradicts (20).

A similar contradiction argument can be applied in the case when the line is congested, meaning $I_\ell > I_\ell^{\max}$. We conclude that the assumption that the sets S and R are both non-empty was invalid, and therefore one set must always be empty, and we reduce to Case I or Case II. ■

REFERENCES

[1] D. E. Olivares *et al.*, "Trends in microgrid control," *IEEE Trans. Smart Grid*, vol. 5, no. 4, pp. 1905–1919, Jul. 2014.

[2] A. Bidram and A. Davoudi, "Hierarchical structure of microgrids control system," *IEEE Trans. Smart Grid*, vol. 3, no. 4, pp. 1963–1976, Dec. 2012.

[3] M. Yazdanian and A. Mehrizi-Sani, "Distributed control techniques in microgrids," *IEEE Trans. Smart Grid*, vol. 5, no. 6, pp. 2901–2909, Nov. 2014.

[4] Q. Shafiee, J. M. Guerrero, and J. C. Vasquez, "Distributed secondary control for islanded microgrids—A novel approach," *IEEE Trans. Power Electron.*, vol. 29, no. 2, pp. 1018–1031, Feb. 2014.

[5] J. W. Simpson-Porco *et al.*, "Secondary frequency and voltage control of islanded microgrids via distributed averaging," *IEEE Trans. Ind. Electron.*, vol. 62, no. 11, pp. 7025–7038, Nov. 2015.

[6] C.-Y. Chang and W. Zhang, "Distributed control of inverter-based lossy microgrids for power sharing and frequency regulation under voltage constraints," *Automatica*, vol. 66, pp. 85–95, Apr. 2016.

[7] T. Zhao and Z. Ding, "Distributed agent consensus-based optimal resource management for microgrids," *IEEE Trans. Sustain. Energy*, vol. 9, no. 1, pp. 443–452, Jan. 2018.

[8] Z. Wang, W. Wu, and B. Zhang, "A fully distributed power dispatch method for fast frequency recovery and minimal generation cost in autonomous microgrids," *IEEE Trans. Smart Grid*, vol. 7, no. 1, pp. 19–31, Jan. 2016.

[9] C. Zhao, J. He, P. Cheng, and J. Chen, "Consensus-based energy management in smart grid with transmission losses and directed communication," *IEEE Trans. Smart Grid*, vol. 8, no. 5, pp. 2049–2061, Sep. 2017.

[10] Y. Xu and Z. Li, "Distributed optimal resource management based on the consensus algorithm in a microgrid," *IEEE Trans. Ind. Electron.*, vol. 62, no. 4, pp. 2584–2592, Apr. 2015.

[11] G. Binetti, A. Davoudi, F. L. Lewis, D. Naso, and B. Turchiano, "Distributed consensus-based economic dispatch with transmission losses," *IEEE Trans. Power Syst.*, vol. 29, no. 4, pp. 1711–1720, Jul. 2014.

[12] Z. Wang, F. Liu, S. H. Low, C. Zhao, and S. Mei, "Distributed frequency control with operational constraints, part I: Per-node power balance," *IEEE Trans. Smart Grid*, vol. 10, no. 1, pp. 40–52, Jan. 2019.

[13] Z. Wang, F. Liu, S. H. Low, C. Zhao, and S. Mei, "Distributed frequency control with operational constraints, part II: Network power balance," *IEEE Trans. Smart Grid*, vol. 10, no. 1, pp. 53–64, Jan. 2019.

[14] P. Yi, Y. Hong, and F. Liu, "Distributed gradient algorithm for constrained optimization with application to load sharing in power systems," *Syst. Control Lett.*, vol. 83, pp. 45–52, Sep. 2015.

[15] W. Zhang, W. Liu, X. Wang, L. Liu, and F. Ferrese, "Online optimal generation control based on constrained distributed gradient algorithm," *IEEE Trans. Power Syst.*, vol. 30, no. 1, pp. 35–45, Jan. 2015.

[16] A. N. M. M. Haque *et al.*, "Integrating direct and indirect load control for congestion management in LV networks," *IEEE Trans. Smart Grid*, vol. 10, no. 1, pp. 741–751, Jan. 2019.

[17] S. S. D. Thukaram, "Network congestion management by fuzzy inference using virtual flows," in *Proc. Int. Conf. Power Energy Syst. (ICPS)*, Dec. 2011, pp. 1–6.

[18] D. B. Nguyen, J. M. Scherpen, and F. Bliek, "Distributed optimal control of smart electricity grids with congestion management," *IEEE Trans. Autom. Sci. Eng.*, vol. 14, no. 2, pp. 494–504, Apr. 2017.

[19] T. H. Vo *et al.*, "A study of congestion management in smart distribution networks based on demand flexibility," in *Proc. IEEE PowerTech*, 2017, pp. 1–6.

[20] S. Huang, Q. Wu, M. Shahidehpour, and Z. Liu, "Dynamic power tariff for congestion management in distribution networks," *IEEE Trans. Smart Grid*, vol. 10, no. 2, pp. 2148–2157, Mar. 2019.

[21] G. De Carne, M. Liserre, K. Christakou, and M. Paolone, "Integrated voltage control and line congestion management in active distribution networks by means of smart transformers," in *Proc. IEEE 23rd Int. Symp. Ind. Electron. (ISIE)*, 2014, pp. 2613–2619.

[22] G. Yu, H. Song, R. Hou, Y. Qu, and H.-M. Kim, "Distributed frequency control strategy for islanded microgrid with consideration of transmission congestion," *Int. J. Smart Home*, vol. 10, no. 6, pp. 309–320, 2016.

[23] C. Zhao, E. Mallada, S. Low, and J. Bialek, "A unified framework for frequency control and congestion management," in *Proc. Power Syst. Comput. Conf. (PSCC)*, Jun. 2016, pp. 1–7.

[24] M. Farivar, R. Neal, C. Clarke, and S. Low, "Optimal inverter VAR control in distribution systems with high PV penetration," in *Proc. IEEE-PES GM*, 2012, pp. 1–7.

[25] W. Ren, R. W. Beard, and E. M. Atkins, "Information consensus in multivehicle cooperative control," *IEEE Control Syst.*, vol. 27, no. 2, pp. 71–82, Apr. 2007.

[26] F. Bullo. (2017). *Lectures on Network Systems, Version 0.95*. [Online]. Available: http://motion.me.ucsb.edu/book-lns

[27] P. Vergara *et al.*, "Distributed strategy for optimal dispatch of unbalanced three-phase islanded microgrids," *IEEE Trans. Smart Grid*, to be published.

[28] Plexim. (2010). *PLECS Software for Power Electronics*. [Online]. Available: http://www.plexim.com

[29] M. Johansson and A. Rantzer, "Computation of piecewise quadratic Lyapunov functions for hybrid systems," *IEEE Trans. Autom. Control*, vol. 43, no. 4, pp. 555–559, Apr. 1998.

[30] J. M. Gonçalves, A. Megretski, and M. A. Dahleh, "Global analysis of piecewise linear systems using impact maps and surface Lyapunov functions," *IEEE Trans. Autom. Control*, vol. 48, no. 12, pp. 2089–2106, Dec. 2003.

Jacqueline Llanos (S'10–M'13) received the B.Sc. degree in electronic engineering from Army Polytechnic School, Ecuador, and the M.Sc. degree in electrical engineering from the University of Chile, Santiago, Chile, where she is currently pursuing the Ph.D. degree.

Her current research interests include control and management of microgrids, control of power generation plants, and predictive control.

Daniel E. Olivares (S'11–M'14) was born in Santiago, Chile. He received the B.Sc. and Engineering degrees in electrical engineering from the University of Chile, Santiago, in 2006 and 2008, respectively, and the Ph.D. degree in electrical and computer engineering from the University of Waterloo, Waterloo, ON, Canada, in 2014.

He is currently an Assistant Professor with the Department of Electrical Engineering, Pontificia Universidad Católica de Chile, Santiago. His research interests include modeling, simulation, and control and optimization of power systems in the context of smart grids.

John W. Simpson-Porco (S'11–M'16) received the B.Sc. degree in engineering physics from Queen's University, Kingston, ON, Canada, in 2010 and the Ph.D. degree in mechanical engineering from the University of California at Santa Barbara, Santa Barbara, CA, USA, in 2015.

He was a Visiting Scientist with the Automatic Control Laboratory, ETH Zurich, Zürich, Switzerland. He is currently an Assistant Professor of electrical and computer engineering with the University of Waterloo, Waterloo, ON, Canada. His research focuses on the control and optimization of multiagent systems and networks, with applications in modernized power grids.

Prof. Simpson-Porco was a recipient of the 2012–2014 IFAC Automatica Prize, the Center for Control, Dynamical Systems and Computation Best Thesis Award, and the Outstanding Scholar Fellowship.

Mehrdad Kazerani (S'88–M'96–SM'02) received the B.Sc. degree in electrical engineering from Shiraz University, Iran, in 1980, the master's degree in electrical engineering from Concordia University, Canada, in 1990, and the Ph.D. degree in electrical engineering from McGill University, Canada, in 1995.

From 1982 to 1987, he was with Energy Ministry of Iran. He is currently a Professor with the Department of Electrical and Computer Engineering, University of Waterloo, Canada. His research interest include current-sourced converter applications, power quality/active power filters, matrix converters, distributed power generation, utility interface of alternative energy sources, energy storage and battery charging systems, battery electric, hybrid electric and fuel cell vehicles, microgrids, HVDC, and flexible ac transmission systems.

Dr. Kazerani is a Registered Professional Engineer in the province of Ontario.

Doris Sáez (S'93–M'96–SM'05) was born in Panguipulli, Chile. She received the M.Sc. and Ph.D. degrees in electrical engineering from the Pontificia Universidad Católica de Chile, Santiago, Chile, in 1995 and 2000, respectively.

She is currently a Full Professor with the Department of Electrical Engineering, University of Chile, Santiago. She has coauthored the books entitled *Hybrid Predictive Control for Dynamic Transport Problems* (Springer-Verlag, 2013) and *Optimization of Industrial Processes at Supervisory Level: Application to Control of Thermal Power Plants* (Springer-Verlag, 2002). Her research interests include predictive control, fuzzy control design, fuzzy identification, control of power generation plants, and control of transport systems. She is an Associate Editor of the IEEE TRANSACTIONS ON FUZZY SYSTEMS and *IEEE Control Systems Magazine*.